On the Potential of Sentinel-2 for Estimating Gross Primary Production

Daniel E. Pabon-Moreno, Mirco Migliavacca, Markus Reichstein, and Miguel D. Mahecha

***Abstract*— Estimating gross primary production (GPP), the gross uptake of CO_2 by vegetation, is a fundamental prerequisite for understanding and quantifying the terrestrial carbon cycle. Over the last decade, multiple approaches have been developed to derive spatiotemporal dynamics of GPP combining *in situ* observations and remote sensing data using machine learning techniques or semiempirical models. However, no high spatial resolution GPP product exists so far that is derived entirely from satellite-based remote sensing data. Sentinel-2 satellites are expected to open new opportunities to analyze ecosystem processes with spectral bands chosen to study vegetation between 10- and 20-m spatial resolutions with five-day revisit frequency. Of particular relevance is the availability of red-edge bands that are suitable for deriving estimates of canopy chlorophyll content that are expected to be much better than any previous global mission. Here, we analyzed whether red-edge-based and near-infrared-based vegetation indices (VIs) or machine learning techniques that consider VIs, all spectral bands, and their nonlinear interactions could predict daily GPP derived from 58 eddy covariance sites. Using linear regressions based on classic VIs, including near-infrared reflectance of vegetation (NIRv), we achieved prediction powers of $R^2_{10-\text{fold}} = 0.51$ and an $\text{RMSE}_{10-\text{fold}} = 2.95$ [µmol CO_2 $m^{-2}s^{-1}$] in a 10-fold cross validation. Chlorophyll index red (CIR) and the novel kernel NDVI (kNVDI) achieved significantly higher prediction powers of around $R^2_{10-\text{fold}} \approx 0.61$ and $\text{RMSE}_{10-\text{fold}} \approx 2.57$ [µmol CO_2 $m^{-2}s^{-1}$]. Using all spectral bands and VIs jointly in a machine learning prediction framework allowed us to predict GPP with $R^2_{10-\text{fold}} = 0.71$ and $\text{RMSE}_{10-\text{fold}} = 2.68$ [µmol CO_2 $m^{-2}s^{-1}$]. Despite the high-power prediction when machine learning techniques are used, under water-stress scenarios or heat waves, optical information alone is not enough to predict GPP properly. In general, our analyses show the potential of nonlinear combinations of spectral bands and VIs for monitoring GPP across ecosystems at a level of accuracy comparable to previous works, which, however, required additional meteorological drivers.**

***Index Terms*— Gross primary production, red edge, Sentinel-2.**

Manuscript received October 13, 2021; revised January 5, 2022; accepted January 17, 2022. Date of publication February 16, 2022; date of current version March 31, 2022. This work was supported by the European Union's Horizon 2020 Research and Innovation Program via the TRuStEE Project through the Marie Skłodowska-Curie Grant under Agreement 721995. *(Corresponding author: Daniel E. Pabon-Moreno.)*

Daniel E. Pabon-Moreno is with the Department of Biogeochemical Integration, Max Planck Institute for Biogeochemistry, 07745 Jena, Germany (e-mail: dpabon@bgc-jena.mpg.de).

Mirco Migliavacca is with the European Commission, Joint Research Centre (JRC), 21027 Ispra, Italy, and also with the Department of Biogeochemical Integration, Max Planck Institute for Biogeochemistry, 07745 Jena, Germany (e-mail: mirco.migliavacca@ec.europa.eu).

Markus Reichstein is with the Department of Biogeochemical Integration, Max Planck Institute for Biogeochemistry, 07745 Jena, Germany, and also with the Michael-Stifel-Center Jena for Data-Driven and Simulation Science, Friedrich-Schiller-University Jena, 07743 Jena, Germany (e-mail: mreichstein@bgc-jena.mpg.de).

Miguel D. Mahecha is with the Remote Sensing Center for Earth System Research, Leipzig University, 04103 Leipzig, Germany, and also with the Helmholtz Centre for Environmental Research, 04318 Leipzig, Germany (e-mail: miguel.mahecha@uni-leipzig.de).

This article has supplementary downloadable material available at https://doi.org/10.1109/TGRS.2022.3152272, provided by the authors.

Digital Object Identifier 10.1109/TGRS.2022.3152272

I. Introduction

GROSS primary production (GPP), the amount of carbon absorbed by the ecosystem via plant photosynthesis, is the largest single flux in the global carbon cycle [1]. GPP varies in response to several abiotic (e.g., radiation, temperature, and precipitation; 2 and 3) and biotic factors (e.g., metabolic pathway, vegetation type, leaf chemical traits, and species composition: 4). However, GPP cannot be directly observed and needs to be derived from *in situ* measurements of net CO_2 exchanges using the eddy covariance (EC) technique over canopies [5], [6]. Using different flux partitioning methods, it is possible to estimate the amount of carbon that is taken up by the ecosystem (GPP) or released through ecosystem respiration (RECO) [7]–[11]. Nevertheless, EC can only measure the exchange of energy and matter between the ecosystem and the atmosphere at the scale of the climatology footprint, which can vary between a few hundred meters to a few kilometers (e.g., 12). Today, EC data are available globally in multiple regional networks (Integrated Carbon Observation System: ICOS, The National Ecological Observatory Network: NEON, AmeriFlux, AsiaFlux) and the meta-network Fluxnet [13], [14]. The flux database networks enable studies into local processes understanding [6], [15]–[17], evaluating biotic and abiotic relationships on multiple time scales (e.g., 18 and 19), and evaluating terrestrial biosphere models [20]–[23].

In the last decades, many process-based, semiempirical, and data-driven models have been developed to upscale GPP using remote sensing data, and climate information, in order to understand the spatiotemporal dynamics of the global carbon cycle [3], [24]–[26]. For instance, the MODIS MOD17 product is based on a semiempirical model that estimates GPP as the product between the light-use efficiency and the absorbed photosynthetically active radiation (APAR) [27]. The maximum light-use efficiency is a plant functional-type-dependent parameter, and it is downregulated by stress factors that depend on temperature and vapor pressure deficit that need to be parameterized. The Breathing Earth System Simulator (BESS) [28] is a process-based approach, which relies on a radiative-transfer model coupled with several remote sensing products to predict GPP and evapotranspiration (ET) at a global scale with a temporal resolution of eight days. Jung *et al.* [29] showed that machine learning methods can likewise efficiently upscale fluxes from *in situ* data to the globe. Building on this work, Tramontana *et al.* [30] used the FLUXNET dataset and MODIS remote sensing information to train multiple machine learning techniques to predict monthly GPP at a global scale. Later, Bodesheim *et al.* [31] produced GPP global products at half-hour temporal resolution using different settings, but of low spatial resolution (0.5°). The state-of-the-art machine learning-based upscaling of GPP is described in [26].

A more direct approach to predicting GPP is to identify vegetation indices that are highly correlated with GPP dynamics. Badgley *et al.* [32], for instance, found that the near-infrared reflectance of vegetation (NIRv) index strongly correlates with monthly estimates of sun-induced chlorophyll fluorescence (SIF), rendering it a potential predictor for GPP at the global scale. Later on, Badgley *et al.* [33] showed that NIRv can explain 68% of the monthly GPP variability at the FLUXNET sites. Recently, Camps-Valls *et al.* [34] presented a nonlinear version of the normalized difference vegetation index (NDVI) based on kernel methods (kNDVI) that correlates better with GPP and SIF products than NIRv and NDVI. The advantage of such approaches is that they rely purely on remote sensing data and circumvent the parameterization of light-use efficiency models. However, relying on reflectance values alone means that the detection of physiological regulation of photosynthesis via meteorological conditions is not detectable unless they last long enough to affect vegetation pigments and structure.

Today, new satellite missions have increased the information available to characterize vegetation properties and ecosystem processes [35], [36]. Specifically, the satellite missions from the Copernicus program have opened new ways to monitor ecosystem processes with unprecedented spatial, temporal, and spectral resolution [37], [38]. For instance, it has been shown that Copernicus missions allow deriving plant traits such as chlorophyll and nitrogen content along with other biophysical parameters [39]–[42]. To the best of our knowledge, only three studies have evaluated the prediction capacities of GPP using Sentinel-2: Wolanin *et al.* [43] used the SCOPE model and machine learning techniques to predict GPP of C3 crops. Lin *et al.* [44] evaluated the potential prediction of GPP as a function of the vegetation index multiplied by the incident photosynthetic active radiation (PARin). They analyzed the performance of five red-edge vegetation indices and three nonred-edge vegetation indices. They found that chlorophyll index red (CIR) showed the highest correlation with GPP from the EC tower for two grassland sites. Finally, Cai *et al.* [45] compared GPP predictions using Sentinel-2 and MODIS for several EC-sites in Northern Europe. The authors did not find any improvement for the prediction of GPP when using Sentinel-2 compared to MODIS using the enhanced vegetation index (EVI2). Despite these advances, there is a lack of systematic comparison between novel red-edge vegetation indices and vegetation indices based on the classic red and NIR bands (i.e., NDVI, kNDVI, and NIRv) in terms of their predictive power regarding GPP. Likewise, the question of whether a machine learning approach considering all Sentinel-2 bands could improve the satellite-based predictions of GPP remains unresolved.

In this study, we aim at understanding the potential of Sentinel-2 mission for monitoring GPP across European and North American major biomes at high spatial resolution. First, we want to understand, which vegetation indices or spectral bands available from Sentinel-2 are the most relevant for predicting GPP. Second, we investigate what is the difference in prediction performance between different approaches based on state-of-the-art vegetation indices (e.g., NIRv, kNDVI, red-edge based, and nonred-edge indices) and machine learning using all spectral bands.

II. Methods

A. Eddy Covariance Sites

We used 58 EC sites compiled by the ICOS Drought 2018 Team (49 sites) and the Ameriflux/ONEFLUX (9 sites) initiatives from 2015 to 2018 (Appendix A). We used half-hourly GPP data (GPP_NT_VUT_USTAR50) estimated using the FLUXNET2015 workflow [14]. GPP is calculated in FLUXNET with the night-time partitioning method [8] using a variable u* threshold for each year. The annual u* threshold is derived from the 50th percentile of u* threshold distribution obtained by bootstrapping the original night-time net ecosystem exchange data [14]. Daily GPP values are estimated as the mean of the half-hourly values where net ecosystem exchange is observed or gap-filled with good quality (e.g., NEE_VUT_USTAR50_QC $= 0$ and 1). In our analysis, days with less than 70% of good quality half-hourly data were set to "NA." Finally, we smoothed the time series using a moving window mean with a window size of seven days.

The EC sites span across Europe and United States from a latitude of 34.3°N to 67.8°N and include a variety of vegetation types: croplands (9 sites), deciduous broadleaf forests (9 sites), evergreen needleleaf forests (18 sites), grasslands (7 sites), mixed forest (4 sites), open shrublands (2 sites), savannas (4 sites), and wetlands (5 sites). The sites' locations represent a variety of climatic regimes, including Mediterranean, humid subtropical, temperate oceanic, humid continental, subarctic, and tundra (Appendix A).

B. Sentinel-2 Imagery

We downloaded Sentinel-2 L1C products for the EC sites from 2015 to 2018 using the Scihub Copernicus portal (https://scihub.copernicus.eu/, last accessed October 2020). We performed atmospheric corrections for all products using Sen2Cor 2.5.5 [46]. All bands were resampled to 20-m resolution using the nearest neighbor approach for upsampling and median for downsampling. Finally, we computed several vegetation indices (see Supplementary Material 9) such as NDVI, kNDVI, NIRv, and multiple red-edge vegetation indices as the inverted red-edge chlorophyll index (IRECI) and CIR. Among these indices, kNDVI requires a specific parameterization of the kernel width σ, which was here set to the median distance between the near-infrared band (NIR) and the red band per spatial pixel; for Sentinel-2, $\sigma = \text{median}(0.5 \times (B8 + B4))$. Postprocessing of the images was performed using SNAP v7.0 [47] and automatized using the graph processing framework and the graph processing tool. The scripts for the postprocessing of the products are available at a Zenodo repository (see code availability).

We defined a buffer area of 100 m radius around the EC towers to ensure that the flux footprint climatology lies within this area (Supplementary Material 1). We used the scene classification generated by Sen2Cor to filter out images with: "no data," "saturated or defective pixels," "dark areas," "cloud shadows," "water," "cloud," "thin cirrus," and "snow." To reduce the effect of shadows or saturated pixels that are not correctly classified by Sen2Cor, we implemented an outlier detection approach that consists of three steps. First, we computed z-scores (data centered and scaled to unit variance) per image and removed pixels of the buffer area with an absolute residual value higher than quantile

0.99 [48]. Second, to detect potential images with clouds, we used the time series of the spectral bands per site. We then estimated the average of the buffer area for each image/band and decomposed the time series of each band into a seasonal and a trend component using locally estimated scatterplot smoothing [LOESS 49]. Next, we applied an inner quantile range technique over the residual of the time series decomposition [50]. Residuals with values higher or lower value than three times the quantiles 0.25 and 0.75, respectively, were also classified as outliers. This analysis was performed using the "anomalize" R package [50]. Third, we defined a bigger buffer area of 900 m, where we estimated the percentage of clouds. We removed observations where the percentage of clouds was above 70%. We also identified 16 additional images with clouds by visual inspection (Supplementary Material 3). We present the complete description of the time series decomposition and the outlier detection in Supplementary Material 2 (the R scripts are available in the Zenodo repository, see code availability). The minimum number of images per site detected as an outlier is 1, the maximum is 20, and the mean across sites is 6 images. Finally, we selected the daily GPP values for the days when we also have valid images from Sentinel-2.

C. Dataset Balancing

The imbalanced representation of different categories in a dataset can influence the weighting of the observations during the training process and consequently in the quality of the prediction [51]. In the last decades, several methods have been developed to solve this issue, mainly for classifications problems, but recently also for regression analysis [52], [53]. To address this problem for the prediction of GPP through different vegetation types that are not all equally represented (Fig. 1), we implemented three methods to balance the dataset given the differences in the number of observations per vegetation type.

1) *Undersampling Balancing:* All observations are grouped by vegetation type and are resampled without replacement, to the number of observations of the vegetation type with the least observations.
2) *Oversampling Balancing:* All observations are again grouped by vegetation type. Each category is completed until reaching the number of observations of the maximum category (sampling with replacement). The replacement technique is only applied when the total observations of the category are less than the difference between the number of observations of the category with the maximum number of observations and the total number of observations of the current vegetation type.
3) *Synthetic Minority Oversampling TEchnique for Regression (SMOTER) Balancing:* It is a balancing technique proposed by Torgo *et al.* [52], where the idea behind the method is to undersample observations with high frequency. In contrast, values with a low frequency (rare observations) are oversampled. In this form, rare observations will have a higher weight during the training. All the following analyzes were applied considering all three balancing techniques as well as to the imbalanced case.

D. Linear Regression-Based GPP Prediction

We evaluated the performance of red-edge vegetation indices to predict GPP using linear regression using the balanced and imbalanced datasets. We compared the performance of NDVI, NIRv, and kNDVI [34], as well as red-edge vegetation indices such as IRECI and CIR (for an overview, see Supplementary Material 9). All evaluations were based on leave-location-and-time-out tenfold cross validation as proposed by Meyer *et al.* [54] and implemented in the "CAST" R package [55]. To increase the robustness of the analysis, the generation of tenfolds was repeated 50 times. In this approach, the partitions for the cross validation are semirandomly generated to minimize spatial and temporal autocorrelation. We evaluated the performances of the different models using the coefficient of determination (R^2) of the linear regression between observed and predicted GPP, the root-mean-square error (RMSE), and the mean absolute error (MAE). Finally, we compared the distributions of the model evaluation metrics between the vegetation indices using the Wilcoxon test [56].

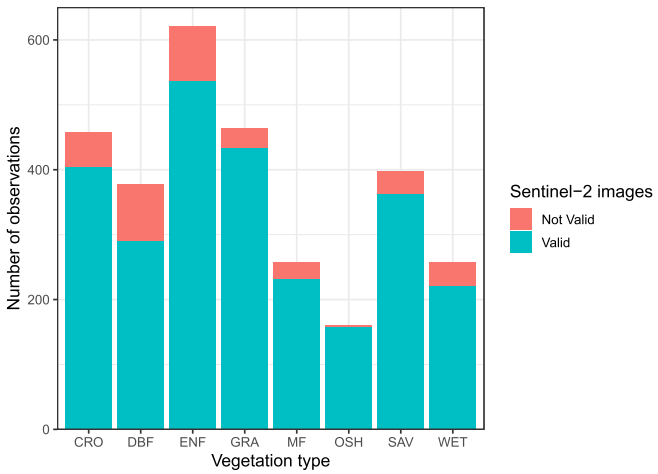

Fig. 1. Number of Sentinel-2 images used for the prediction of GPP (2015–2018) per vegetation type. Each observation corresponds to a Sentinel-2 image at a 100 m radius around the EC tower. Red color indicates the images with no data, saturated or defective pixels, dark areas, cloud shadows, water, clouds, thin cirrus, or snow effects that were removed. Blue color represents the number of valid images. Evergreen needleleaf forests (ENF), croplands (CRO), deciduous broadleaf forests (DBF), grasslands (GRA), wetlands (WET), mixed forest (MF), savannas (SAV), and open shrublands (OSH).

E. Machine Learning-Based GPP Prediction

We used random forests [57] as prediction approach for GPP for each balanced and imbalanced dataset. A detailed description of how to use RF for upscaling land surface fluxes can be found in [31]. We explored what variables are the most relevant for predicting GPP. For this, we evaluated the radiometric indices presented in Supplementary Material 9, additionally to the spectral bands B1, B2, B3, B4, B5, B6, B7, B8, B8A, B9, B11, and B12 (Supplementary Material 8) resulting in a total of 35 predictor variables. kNDVI was not included here since it is a nonlinear transformation of the NDVI using kernel methods, and its inclusion would have added no information when applying machine learning techniques. We performed a forward feature selection as suggested by Meyer *et al.* [58], where the models are generated based on the pairs' combination of predictors, allowing us here to compare nonlinear combinations of spectral bands and vegetation indices, as we may expect that they could reduce model complexity. The power prediction of each model was estimated using a tenfold leave-location-and-time-out cross validation [54], where the tenfolds were generated 50 times to increase the robustness

of the analysis. The idea is that the model with highest R^2 is selected first, and then, new variables are iteratively added to this initial model. The process finishes when none of the remaining variables increases model performance.

III. Results and Discussion

In the following, we first report the results of the GPP prediction using different vegetation indices in linear regressions, where we specifically discuss the performance of GPP estimates based on red-edge vegetation indices compared with the ones based on NIRv, NDVI, and kNDVI. We also discuss the effect of the balancing techniques on the performance of the prediction. Second, we present the results of the GPP prediction using Sentinel-2 spectral bands and vegetation indices using random forests, where we present examples of the prediction for different EC sites and an entire Sentinel-2 tile. Finally, we discuss the possibilities and limitations of predicting GPP using remote sensing information only and how such prediction can be improved in the future and provide globally continuous flux estimates.

A. GPP Prediction Using Linear Regressions

In Fig. 2, we compare the performance of linear GPP predictions using red-edge-based vegetation indices (CIR and IRECI, see Supplementary Material 9), NIRv, NDVI, and kNDVI. Red-edge vegetation indices perform better than NDVI and NIRv in all considered metrics (Fig. 2), while kNDVI performs as well as IRECI. According to the Wilcoxon test, the differences in the performance distribution of each index are statistically significant. In general, CIR explains on average 3% more of the GPP variance than kNDVI, 4% more than IRECI, 10% more than NIRv, and 11% more variance than NDVI. kNDVI explains an average 1% more than IRECI, 7% more than NIRv, and 8% more than NDVI. The prediction of GPP using IRECI shows that 6% more variance in GPP is explained compared to NIRv and 7% more than NDVI. NIRv only explains 1% more of the GPP variance than NDVI. The RMSE shows smaller errors in GPP estimated with CIR, kNDVI, and IRECI compared to the estimates based on NIRv and NDVI (Fig. 2). As expected, when balanced datasets are used, the explained variance increases 2% for CIR, from 2% to 4% for IRECI, from 2% to 5% for NIRv, from 1% to 3% for kNDVI, and from 2% to 3% for NDVI (Table I and Supplementary Material 4).

Badgley *et al.* [32] introduced the NIRv as an alternative to SIF for the estimation of monthly GPP. Compared to machine learning products or radiative-transfer models, the advantage of this approach is that it could be used to estimate global GPP easily using global and long-term time series products such as MODIS. However, our results suggest that the red-edge vegetation index CIR yields significantly higher prediction powers of GPP compared to NIRv. This finding could be interpreted as an important argument for relying on the novel Sentinel-2 data for GPP prediction.

Red edge is the region around 710 nm, which marks the sharp transition between the red region (700 nm), where the absorption of chlorophyll occurs, and the near-infrared region (730 nm), where the reflectance is produced by the internal structures of the leaf [59, p. 180]. This region is highly sensitive to the leaf chlorophyll content [60], [61]. At the same time, chlorophyll content is a controlling factor of the fraction of photosynthetically active radiation absorbed by plants (APAR). This is one possible explanation why CIR is strongly correlated with GPP [62], even if it cannot reflect the fast variations of the photosynthesis itself. For these reasons, VIs based on red-edge bands might generally have advantages for estimating GPP over VIs that do not rely on the red edge. Lin *et al.* [44] found that CIR multiplied by PAR can explain slightly more variability of GPP than NIRv multiplied by PAR for two grasslands sites. However, we would argue that the PAR effect could be dominant in their study, while our aim here was to focus on the spectral information only.

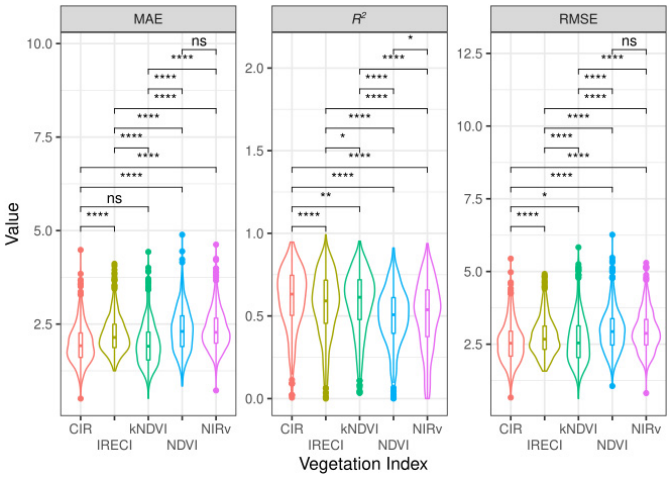

Fig. 2. Prediction of GPP using linear regression and different vegetation indices (CIR: chlorophyll index red, IRECI: inverted red-edge chlorophyll index, NIRv: near-infrared vegetation, and NDVI: normalized difference vegetation index) as predictors. Results are shown for the imbalanced (original) dataset only. The vertical lines correspond to the results of the Wilcoxon test in pairs, where ns is the nonsignificant differences, *: $p \leq 0.05$, **: $p \leq 0.01$, and ***: $p \leq 0.001$.

We also tested the predictive performance of kNDVI [34], which was reported to predict monthly GPP better than NIRv. The idea behind kNDVI is to solve the saturation problem of NDVI at high values by exploring the nonlinear relations of the two bands of the NDVI. Even though no red-edge information is used, we found that kNDVI performed at the level of IRECI in our study. One interpretation of this finding is that most of the information contained in the red-edge bands can be captured by an appropriate transformation of the distance between near-infrared and red bands. However, there is no direct mechanistic argument, and it is unclear to what extent this observation is general and further research will be necessary. However, our results may imply that kernel versions of classical vegetation indices could derive relevant information from satellite missions that do not have red-edge indices.

B. GPP Prediction Using Random Forest

Another question of this study was whether machine learning could outperform even the new generation of vegetation indices. In Table II, we present the results of the variable selection analysis where a different number of predictors are selected depending on the balancing technique. From 35 predictors that included Sentinel-2 spectral bands (Supplementary Material 8) and derived vegetation indices (Supplementary Material 9), CIR, S2REP, and B1 are selected for all datasets, while GNDVI, PSSRA B3, and B4 are selected at least in three cases. ARVI, MTCI, MCARI, B2, and B5 are selected at least in two datasets. IRECI, NDI45, RVI, TNDVI, TSAVI,

TABLE I

AVERAGE PERFORMANCE OF THE GPP PREDICTION USING LINEAR REGRESSION (TENFOLD TEMPORAL–SPATIAL CROSS VALIDATION) WITH RED-EDGE AND NONRED-EDGE VEGETATION INDICES. THE COLUMN DATASET REFERS TO THE BALANCING TECHNIQUE USED TO BALANCE THE REPRESENTATION OF DIFFERENT VEGETATION TYPES

	Red-edge Vegetation indices						Non Red-edge vegetation indices								
	IRECI			CIR			NIRv			NDVI			kNDVI		
Dataset	R^2	RMSE	MAE	R^2	RMSE	MAE	R^2	RMSE	MAE	R^2	RMSE	MAE	R^2	RMSE	MAE
Imbalanced	0.57	2.77	2.23	**0.61**	2.57	1.98	0.51	2.95	2.36	0.50	2.98	2.34	0.58	2.65	1.97
Undersampling	0.61	2.51	2.05	**0.62**	2.43	1.91	0.56	2.70	2.15	0.53	2.84	2.31	0.61	2.48	1.91
Oversampling	0.59	2.63	2.09	**0.61**	2.51	1.93	0.53	2.80	2.20	0.50	2.95	2.36	0.59	2.59	1.94
SMOTER	0.60	3.29	2.75	**0.62**	3.19	2.64	0.55	3.45	2.84	0.52	3.74	3.07	0.54	3.53	2.83

TABLE II

VARIABLES SELECTED FOR THE PREDICTION OF GPP USING THE FORWARD FEATURE SELECTION PRESENTED BY MEYER *et al.* [58]. THE DATASET COLUMN REPRESENTS THE BALANCING TECHNIQUE USED TO BALANCE THE DIFFERENT VEGETATION TYPES IN THE ORIGINAL (IMBALANCED) DATASET. A TENFOLD CROSS VALIDATION IS PERFORMED TO ESTIMATE: R^2, RMSE, AND MAE. THE OPTIMUM NUMBER OF VARIABLES RANDOMLY SAMPLED AS CANDIDATES FOR EACH SPLIT (MTRY) IS ALSO SHOWN. THE INCREASE OF R^2 AND THE DECREASE IN THE STANDARD ERROR WHEN EACH VARIABLE IS ADDED TO THE INITIAL MODEL ARE SHOWN, WHERE THE FIRST VALUE CORRESPONDS TO THE MODEL USING THE FIRST TWO PREDICTORS IN THE COLUMN VARIABLES SELECTED AND THE LAST VALUE CORRESPONDS TO THE VALUE OF THE FINAL MODEL. RED-EDGE CHLOROPHYLL INDEX (CIR), SENTINEL-2 RED-EDGE POSITION INDEX (S2REP), ATMOSPHERICALLY RESISTANT VEGETATION INDEX (ARVI), MERIS TERRESTRIAL CHLOROPHYLL INDEX (MTCI), GREEN NORMALIZED DIFFERENCE VEGETATION INDEX (GNDVI), TRANSFORMED NORMALIZED DIFFERENCE VEGETATION INDEX (TNDVI), NORMALIZED DIFFERENCE INDEX 45 (NDI45), INFRARED PERCENTAGE VEGETATION INDEX (IPVI), PIGMENT SPECIFIC SIMPLE RATIO (PSSRA), TRANSFORMED SOIL ADJUSTED VEGETATION INDEX (TSAVI), MODIFIED CHLOROPHYLL ABSORPTION RATIO INDEX (MCARI), AND GREEN CHLOROPHYLL INDEX (CIG)

Dataset	Number of observations	Number of variables selected	$R^2_{10-fold}$ final model	$RMSE_{10-fold}$ final model	$MAE_{10-fold}$ final model	mtry	Variables selected	$R^2_{10-fold}$	Standard Error
Imbalanced	2636	9	0.66	2.34	1.76	2	CIR, B1	0.593	0.008
							B3	0.632	0.008
							B4	0.649	0.008
							B2	0.653	0.008
							B5	0.655	0.008
							PSSRA	0.655	0.008
							S2REP	0.657	0.008
							GNDVI	0.659	0.007
Undersampling	1264	12	0.68	2.20	1.68	2	CIR, B1	0.620	0.010
							B5	0.652	0.009
							TNDVI	0.664	0.009
							PSSRA	0.669	0.009
							NDVI45	0.671	0.009
							GNDVI	0.671	0.009
							IRECI	0.671	0.009
							MTCI	0.673	0.009
							RVI	0.674	0.009
							S2REP	0.674	0.009
							ARVI	0.675	0.009
Oversampling	4288	9	0.67	2.28	1.70	2	CIR, B1	0.582	0.008
							B3	0.632	0.008
							B4	0.656	0.007
							GNDVI	0.661	0.007
							PSSRA	0.665	0.007
							S2REP	0.668	0.007
							MCARI	0.669	0.007
							ARVI	0.670	0.007
SMOTER	2635	11	0.71	2.68	2.10	2	CIR, B4,	0.635	0.009
							B3	0.664	0.009
							B2	0.685	0.008
							MTCI	0.690	0.008
							S2REP	0.697	0.008
							B12	0.700	0.008
							B1	0.702	0.008
							TSAVI	0.703	0.008
							MCARI	0.705	0.008
							CIG	0.706	0.008

CIG, and B12 are selected at least once (Table II). The variable selection analysis shows that even when nonlinear combinations of spectral bands are possible, vegetation indices are still selected as they probably would simplify the machine learning model. Yet, not all information required for predicting GPP seems to be encoded in vegetation indices alone. Bands B1, B2, B3, B4, B5, and B12 also appear to provide information that is useful for the predictions. A surprising result is the selection of band B1. This band is typically used for aerosol detection and correction purposes. We speculate that B1 is a proxy for radiation dynamics (e.g., direct and diffuse radiation) that are important for GPP. However, we note that Penuelas *et al.* [63] had considered this spectral region earlier in their structure insensitive pigment index (SIPI)

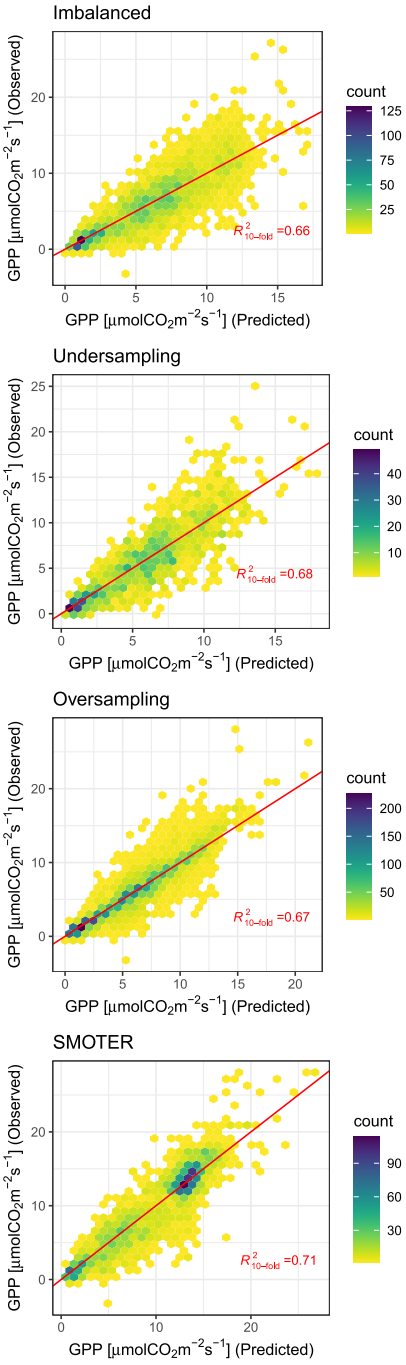

Fig. 3. Prediction of GPP using different data balancing techniques. In each case, the observed values are shown on the y-axis, and the predicted values are shown on the x-axis. The red line represents the 1:1 line. Imbalanced makes reference to the original dataset. Undersampling, oversampling, and SMOTER make reference to each technique used to balance the dataset (see Section II for further details).

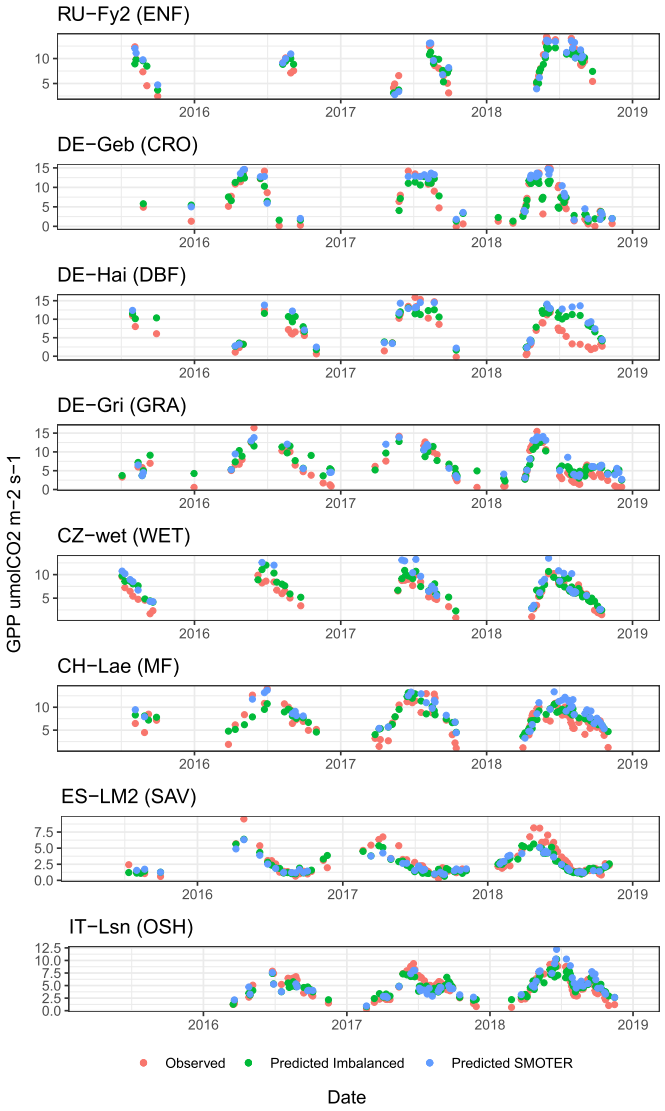

Fig. 4. Observed and predicted GPP values at selected EC sites representing different vegetation types: evergreen needleleaf forests (ENF), croplands (CRO), deciduous broadleaf forests (DBF), grasslands (GRA), wetlands (WET), mixed forest (MF), savannas (SAV), and open shrublands (OSH). Models were trained using a leave-one-site-out cross-validation strategy.

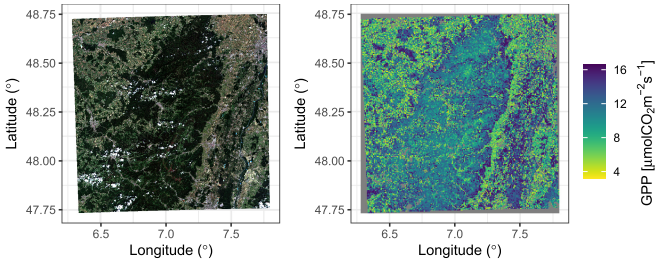

Fig. 5. GPP product for a Sentinel-2 tile, over the Ballons des Vosges Regional Nature Park (France, June 23, 2020). The land cover classification generated by Sen2cor was applied before the prediction, where pixels considered as nonvegetation are encoded as NAs.

that has, however, not been developed further for vegetation monitoring. The additional selection of bands B2 (blue), B3 (green), B4 (red), and B5 (vegetation red-edge) suggests that there is space for the development of new vegetation indices that can capture the GPP variability beyond the existing indices.

In Fig. 3, we present the prediction of GPP using random forest regression, where GPP can be predicted with $R^2_{10-\text{fold}} = 0.66$ and $\text{RMSE}_{10-\text{fold}} = 2.34$ [μmol CO_2 $m^{-2}s^{-1}$] for the imbalanced dataset. There are improvements in the variance explained using the balanced dataset. $R^2_{10-\text{fold}} = 0.68$ and $\text{RMSE}_{10-\text{fold}} = 2.20$ [μmol CO_2 $m^{-2}s^{-1}$]

using undersampling, $R^2_{10-\text{fold}} = 0.67$ and $\text{RMSE}_{10-\text{fold}} = 2.28$ [μmol CO_2 $m^{-2}s^{-1}$] using oversampling technique, and $R^2_{10-\text{fold}} = 0.71$ and $\text{RMSE}_{10-\text{fold}} = 2.68$ [μmol CO_2 $m^{-2}s^{-1}$] using the SMOTER technique (Table II). The comparison between the distribution of the metrics shows that there are significant differences between the imbalanced and balanced datasets (Supplementary Material 10). The results of the cross validation for each fold and balancing technique are presented in Supplementary Material 7. Tramontana *et al.* [30] reported that spectral information with machine learning techniques can explain around 78% of the GPP variability across sites. One of the advantages of our approach is that it does not require a previous vegetation-type classification [64]. In comparison with the estimation of GPP using biophysical parameters as, e.g., in [44], we show that it GPP can be estimated more directly with high accuracy.

In Fig. 4, we present the examples of predicted and observed GPP representing different vegetation types. The prediction for each site is presented in Supplementary Material 5. Despite the overall high variances explained by random forests, there are indeed cases when GPP cannot be predicted correctly. For instance, the maximum GPP is underestimated in savannas and evergreen needleleaf forest ecosystems. Our study period covers the 2018 heat wave, an extreme event where northwestern Europe vegetation was highly affected [65]–[67]. We find, however, that the reduction in CO_2 uptake during this event was not well captured for mixed forest and deciduous broadleaf forest (Fig. 4). This can also be seen when comparing the time series of 2016 and 2017 to 2018 (see Fig. 4). This means that the prediction of ecosystem fluxes during extreme events remains an open issue that needs to be addressed with high priority as discussed in [68]. However, our finding that GPP dynamics during drought events cannot be well represented is in-line with earlier findings. For instance, Bodesheim *et al.* [31] showed that GPP was not properly predicted during dry summers for several EC sites and attributed this to the poor representation of water availability in their dataset. Different from our study, their study also used climate information, which, in theory, increases the model performance for water-stress scenarios. One general problem could be the time lag between the change of photosynthesis rates and the decline in the concentration of the pigments, including chlorophyll content, in the leaves. However, given that the data generated here are based on vegetation reflectance properties only, it is expected that they can only pick up changes in GPP that are primarily driven by changes in APAR and pigment concentrations but are not apt to capture the fast response of photosynthesis mediated, e.g., by stomatal closure. This limitation is inherent to all reflectance-based methods and the reason why, in some sites, we are not able to reproduce GPP dynamics under stress.

Nevertheless, the overall seasonal dynamics are represented very well in our GPP estimates across sites and vegetation types. Future studies should investigate whether the inclusion of thermal information from Sentinel-3 or radar information from Sentinel-1 can help to indirectly address the water deficit in the ecosystems during drought periods [69] and lead to the next generation of operational GPP products based on remote sensing data only. In addition, the unique combination of red-edge vegetation indices in Sentinel-2, radar information from Sentinel-1, or multispectral and thermal information from the bands available in Sentinel-3 may open unprecedented possibilities for vegetation monitoring in the near future [35].

Previous studies used plant functional classes as a spatial feature to upscale GPP [30], [70]. To use vegetation types as a predictor of GPP, a necessary step will be to improve the land cover maps to match the resolution of Sentinel-2. The ESA WorldCover consortium gave the first steps, producing the first global land cover map at 10-m resolution for 2020 using radar information from Sentinel-1 and optical information from Sentinel-2 [71]. Future research will have to test the added value of these upcoming products for predicting carbon fluxes at high spatial resolution.

To give a taste of what the mapping of carbon fluxes might look like in the future, in Fig. 5, we present an example of the upscaling of GPP for a Sentinel-2 tile over the Ballons des Vosges Regional Nature Park (France, June 23, 2020; Supplementary Material 6). The area contains different types of deciduous broadleaf forest, weatlands, grasslands, and croplands. Even though our model does not use vegetation type as a predictor, it does clearly differentiate GPP dynamics of crops, weatlands, and forests. The high spatial resolution of Sentinel-2 could be a nice avenue to monitor forests with a high degree of fragmentation [72] or even green areas in cities [73]. A tutorial of how to use the final models produced in our study to upscale GPP using any Sentinel-2 L2A product provided by Copernicus-ESA is presented in the code repository.

IV. Conclusion

In this study, we explore how remote sensing information provided by Sentinel-2 can be used to predict GPP across a variety of vegetation types. We find that the CIR explains an average 10% more of the variability of GPP at daily scale than NIRv and 11% more than NDVI using linear regressions. The high correspondence between kNDVI and IRECI is unanticipated and requires further physical exploration. The prediction power of vegetation indices can be slightly outperformed using machine learning: using random forests, the spectral information provided by Sentinel-2 alone can predict an average 68% of GPP variability (cross-validated). However, under extreme climate conditions such as the 2018 drought/heat wave, meteorological data or thermal information might be necessary to improve the prediction of short-term reduction of GPP that is not associated with changes in APAR or the decline of chlorophyll content. From a methodological point of view, we also explored whether balancing techniques can help to represent vegetation types and rare observations. Furthermore, we found that improvements in the prediction accuracy of GPP are associated with the use of balanced datasets for training. Overall, our study presents a first attempt to assess the capability of Sentinel-2 data alone to predict GPP. Despite the discussed limitations, Sentinel-2 generally offers a highly relevant perspective to map fluxes at high spatial resolution, opening new ways to understand ecosystem processes and responses from local to global scale.

APPENDIX A: EDDY COVARIANCE SITES

SITES FROM THE ICOS DROUGHT 2018 TEAM AND ONEFLUX INITIATIVES USED IN THIS STUDY. THE NUMBER OF OBSERVATIONS CORRESPONDS TO THE NUMBER OF VALID SENTINEL-2 IMAGES RECOVERED FOR THE SITE DURING THE TIME PERIOD. THE VEGETATION TYPE FOR EACH SITE IS PRESENTED: MF = MIXED FORESTS, CRO = CROPLANDS, GRA = GRASSLANDS, ENF = EVERGREEN NEEDLELEAF FORESTS, DBF = DECIDUOUS BROADLEAF FORESTS, WET = WETLANDS, SAV = SAVANNAS, AND OSH = OPEN SHRUBLANDS

Site name	Vegetation type	Number of observations	Years	DOI	Reference
BE-Bra	MF	56	2015-2018	https://doi.org/10.18160/F738-634R	[74]
BE-Lon	CRO	21	2015-2018	https://doi.org/10.18160/6SM0-NFES	[75]
BE-Vie	MF	12	2016-2018	https://doi.org/10.18160/MK3Q-BBEK	[76]
CH-Aws	GRA	31	2016-2018	https://doi.org/10.18160/3YQE-7BR8	NA
CH-Cha	GRA	98	2015-2018	https://doi.org/10.18160/GMMW-5E2D	[77]
CH-Dav	ENF	13	2015-2018	https://doi.org/10.18160/R86M-H3HX	[78]
CH-Fru	GRA	79	2015-2018	https://doi.org/10.18160/J938-0MKS	[79]
CH-Lae	MF	80	2015-2018	https://doi.org/10.18160/FABD-SVJJ	[80]
CH-Oe2	CRO	44	2015-2018	https://doi.org/10.18160/N01Y-R7DF	[81]
CZ-BK1	ENF	22	2015-2018	https://doi.org/10.18160/7QXR-AYEE	[82]
CZ-Lnz	MF	84	2015-2018	https://doi.org/10.18160/84SN-YBSD	NA
CZ-RAJ	ENF	50	2015-2018	https://doi.org/10.18160/HFS9-JBTG	NA
CZ-Stn	DBF	22	2015-2018	https://doi.org/10.18160/V2JN-DQPJ	NA
CZ-wet	WET	68	2015-2018	https://doi.org/10.18160/W4YS-463W	[83]
DE-Akm	WET	39	2015-2018	https://doi.org/10.18160/24B5-J44F	NA
DE-Geb	CRO	60	2015-2018	https://doi.org/10.18160/ZK18-3YW3	[84]
DE-Gri	GRA	73	2015-2018	https://doi.org/10.18160/EN60-T3FG	[85]
DE-Hai	DBF	48	2015-2018	https://doi.org/10.18160/D4ET-BFPS	[86]
DE-HoH	DBF	37	2015-2018	https://doi.org/10.18160/J1YB-YEHC	NA
DE-Hte	WET	44	2015-2018	https://doi.org/10.18160/J1YB-YEHC	NA
DE-Hzd	DBF	28	2015-2018	https://doi.org/10.18160/PJEC-43XB	NA
DE-Kli	CRO	56	2015-2018	https://doi.org/10.18160/STT9-TBJZ	[85]
DE-Obe	ENF	6	2015-2018	https://doi.org/10.18160/FSM3-RC5F	NA
DE-RuR	GRA	39	2015-2018	https://doi.org/10.18160/HPV9-K8R1	[87]
DE-RuS	CRO	28	2015-2018	https://doi.org/10.18160/A2TK-QD5U	[88]
DE-RuW	ENF	20	2015-2018	https://doi.org/10.18160/H7Y6-2R1H	NA
DE-Tha	ENF	45	2015-2018	https://doi.org/10.18160/BSE6-EMVJ	[89]
DK-Sor	DBF	53	2015-2018	https://doi.org/10.18160/BFDT-7HYE	[90]
ES-Abr	SAV	171	2015-2018	https://doi.org/10.18160/11TP-MX4F	[91]
ES-LM1	SAV	80	2015-2018	https://doi.org/10.18160/FDSD-GVRS	[92]
ES-LM2	SAV	92	2015-2018	https://doi.org/10.18160/3SVJ-XSB7	[92]
FI-Hyy	ENF	22	2015-2018	https://doi.org/10.18160/0JHQ-BZMU	
FI-Let	ENF	17	2017-2018	https://doi.org/10.18160/0JHQ-BZMU	[93]
FI-Sii	WET	23	2016-2018	https://doi.org/10.18160/0RE3-DTWD	NA
FI-Var	ENF	38	2016-2018	https://doi.org/10.18160/NYH7-5JEB	NA
FR-EM2	CRO	59	2017-2018	https://doi.org/10.18160/HC1V-8VKJ	NA

(Continued.) SITES FROM THE ICOS DROUGHT 2018 TEAM AND ONEFLUX INITIATIVES USED IN THIS STUDY. THE NUMBER OF OBSERVATIONS CORRESPONDS TO THE NUMBER OF VALID SENTINEL-2 IMAGES RECOVERED FOR THE SITE DURING THE TIME PERIOD. THE VEGETATION TYPE FOR EACH SITE IS PRESENTED: MF = MIXED FORESTS, CRO = CROPLANDS, GRA = GRASSLANDS, ENF = EVERGREEN NEEDLELEAF FORESTS, DBF = DECIDUOUS BROADLEAF FORESTS, WET = WETLANDS, SAV = SAVANNAS, AND OSH = OPEN SHRUBLANDS

FR-Hes	DBF	76	2015-2018	https://doi.org/10.18160/WTYC-JVQV	NA
IT-BCi	CRO	38	2015-2018	https://doi.org/10.18160/T25N-PD1H	[94]
IT-Lsn	OSH	113	2016-2018	https://doi.org/10.18160/RTKZ-VTDJ	NA
IT-Tor	GRA	68	2015-2018	https://doi.org/10.18160/ERMH-PSVW	[95]
NL-Loo	ENF	43	2015-2018	https://doi.org/10.18160/MV3K-WM09	[96]
RU-Fy2	ENF	44	2015-2018	https://doi.org/10.18160/WEV2-WQXY	[97]
RU-Fyo	ENF	46	2015-2018	https://doi.org/10.18160/4J2N-DY7S	[98]
SE-Deg	WET	46	2015-2018	https://doi.org/10.18160/0T47-MEEU	NA
SE-Htm	ENF	35	2015-2018	https://doi.org/10.18160/17FF-96RT	NA
SE-Lnn	CRO	45	2015-2018	https://doi.org/10.18160/5GZQ-S6Z0	NA
SE-Nor	ENF	37	2015-2018	https://doi.org/10.18160/K57M-TVGE	NA
SE-Ros	ENF	58	2015-2018	https://doi.org/10.18160/ZF2F-82Q7	NA
SE-Svb	ENF	38	2015-2018	https://doi.org/10.18160/X57W-HWTE	NA
US-ARM	CRO	53	2016-2018	https://doi.org/10.17190/AMF/1246027	[99]
US-Bar	DBF	4	2016-2018	https://doi.org/10.17190/AMF/1246030	[100]
US-Ho1	ENF	14	2015-2018	https://doi.org/10.17190/AMF/1246061	[101]
US-MMS	DBF	8	2015-2018	https://doi.org/10.17190/AMF/1246080	[102]
US-Seg	GRA	45	2015-2018	https://doi.org/10.17190/AMF/1246124	[103]
US-Ses	OSH	45	2016-2017	https://doi.org/10.17190/AMF/1246125	[104]
US-UMB	DBF	14	2015-2017	https://doi.org/10.17190/AMF/1246107	[105]
US-Vcm	ENF	10	2016-2017	https://doi.org/10.17190/AMF/1246121	[106]
US-Wjs	SAV	20	2015-2017	https://doi.org/10.17190/AMF/1246120	[107]

CODE AVAILABILITY

Code is available under GPL-3 license at: https://github.com/dpabon/Sentinel-2_GPP.

DATA AVAILABILITY

ICOS data are available on the web-site: https://www.icos-cp.eu/data-products/YVR0-4898. Ameriflux data are available on the website: https://ameriflux.lbl.gov/data/download-data-oneflux-beta/.

ACKNOWLEDGMENT

Markus Reichstein and Miguel D. Mahecha thank the European Space Agency for funding the project DeepExtremes-AI for Science, Multi-Hazards, Compounds and Cascade events. This work used eddy covariance data acquired and shared by Ameriflux, and the Integrated Carbon Observation System (ICOS). In addition, funding for AmeriFlux data resources was provided by the U.S. Department of Energy's Office of Science. The authors thank Prof. Dr. Gustau Camps-Valls for his feedback on kNDVI.

REFERENCES

[1] F. S. Chapin *et al.*, "Reconciling carbon-cycle concepts, terminology, and methods," *Ecosystems*, vol. 9, no. 7, pp. 1041–1050, Nov. 2006.

[2] A. D. Richardson, D. Y. Hollinger, J. D. Aber, S. V. Ollinger, and B. H. Braswell, "Environmental variation is directly responsible for short- but not long-term variation in forest-atmosphere carbon exchange," *Global Change Biol.*, vol. 13, no. 4, pp. 788–803, Jan. 2007.

[3] C. Beer *et al.*, "Terrestrial gross carbon dioxide uptake: Global distribution and covariation with climate," *Science*, vol. 329, pp. 834–838, Aug. 2010.

[4] T. Musavi *et al.*, "Stand age and species richness dampen interannual variation of ecosystem-level photosynthetic capacity," *Nature Ecol. Evol.*, vol. 1, no. 2, pp. 1–7, Jan. 2017.

[5] D. D. Baldocchi, "Assessing the eddy covariance technique for evaluating carbon dioxide exchange rates of ecosystems: Past, present and future," *Global Change Biol.*, vol. 9, no. 4, pp. 479–492, Apr. 2003.

[6] D. D. Baldocchi *et al.*, "Outgoing near-infrared radiation from vegetation scales with canopy photosynthesis across a spectrum of function, structure, physiological capacity, and weather," *J. Geophys. Res., Biogeosci.*, vol. 125, no. 7, Jul. 2020, Art. no. e2019JG005534.

[7] E. Falge *et al.*, "Seasonality of ecosystem respiration and gross primary production as derived from FLUXNET measurements," *Agricult. Forest Meteorol.*, vol. 113, nos. 1–4, pp. 53–74, Dec. 2002.

[8] M. Reichstein *et al.*, "On the separation of net ecosystem exchange into assimilation and ecosystem respiration: Review and improved algorithm," *Global Change Biol.*, vol. 11, no. 9, pp. 1424–1439, Sep. 2005.

[9] G. Lasslop *et al.*, "Separation of net ecosystem exchange into assimilation and respiration using a light response curve approach: Critical issues and global evaluation," *Global Change Biol.*, vol. 16, no. 1, pp. 187–208, Jan. 2010.

[10] T. F. Keenan *et al.*, "Widespread inhibition of daytime ecosystem respiration," *Nature Ecol. Evol.*, vol. 3, no. 3, pp. 407–415, Mar. 2019.

[11] G. Tramontana *et al.*, "Partitioning net carbon dioxide fluxes into photosynthesis and respiration using neural networks," *Global Change Biol.*, vol. 26, no. 9, pp. 5235–5253, 2020.

[12] M. Aubinet, T. Vesala, and D. Papale, Eds., *Eddy Covariance: A Practical Guide to Measurement and Data Analysis* (Springer Atmospheric Sciences). Amsterdam, The Netherlands: Springer, 2012.

[13] D. Baldocchi *et al.*, "FLUXNET: A new tool to study the temporal and spatial variability of ecosystem-scale carbon dioxide, water vapor, and energy flux densities," *Bull. Amer. Meteorol. Soc.*, vol. 82, no. 82, pp. 2415–2434, 2001.

[14] G. Pastorello *et al.*, "The FLUXNET2015 dataset and the ONEFlux processing pipeline for eddy covariance data," *Sci. Data*, vol. 7, no. 1, pp. 1–27, 2020.

[15] D. Baldocchi, "'Breathing' of the terrestrial biosphere: Lessons learned from a global network of carbon dioxide flux measurement systems," *Austral. J. Botany*, vol. 56, no. 1, pp. 1–26, Feb. 2008.

[16] D. E. Pabon-Moreno, T. Musavi, M. Migliavacca, M. Reichstein, C. Römermann, and M. D. Mahecha, "Ecosystem physio-phenology revealed using circular statistics," *Biogeosciences*, vol. 17, no. 15, pp. 3991–4006, Aug. 2020.

[17] M. Migliavacca *et al.*, "The three major axes of terrestrial ecosystem function," *Nature*, vol. 598, no. 7881, pp. 468–472, Oct. 2021.

[18] M. D. Mahecha *et al.*, "Characterizing ecosystem-atmosphere interactions from short to interannual time scales," *Biogeosciences*, vol. 4, no. 5, pp. 743–758, Sep. 2007.

[19] C. Krich *et al.*, "Estimating causal networks in biosphere–atmosphere interaction with the PCMCI approach," *Biogeosciences*, vol. 17, no. 4, pp. 1033–1061, Feb. 2020.

[20] A. D. Friend *et al.*, "FLUXNET and modelling the global carbon cycle," *Global Change Biol.*, vol. 13, no. 3, pp. 610–633, Mar. 2007.

[21] M. D. Mahecha *et al.*, "Comparing observations and process-based simulations of biosphere-atmosphere exchanges on multiple timescales," *J. Geophys. Res., Biogeosci.*, vol. 115, no. G2, Jun. 2010, Art. no. G02003.

[22] G. B. Bonan *et al.*, "Improving canopy processes in the community land model version 4 (CLM4) using global flux fields empirically inferred from FLUXNET data," *J. Geophys. Res.*, vol. 116, no. G2, 2011, Art. no. G02014.

[23] M. Sjöström *et al.*, "Evaluation of MODIS gross primary productivity for Africa using eddy covariance data," *Remote Sens. Environ.*, vol. 131, pp. 275–286, Apr. 2013.

[24] F. A. Heinsch *et al.*, *Users Guide: GPP and NPP (MOD17A2/A3) Products NASA MODIS Land Algorithm*. Missoula, MT, USA: Univ. Montana, 2003.

[25] Y. Ryu, J. A. Berry, and D. D. Baldocchi, "What is global photosynthesis? History, uncertainties and opportunities," *Remote Sens. Environ.*, vol. 223, pp. 95–114, Mar. 2019.

[26] M. Jung *et al.*, "Scaling carbon fluxes from eddy covariance sites to globe: Synthesis and evaluation of the FLUXCOM approach," *Biogeosciences*, vol. 17, no. 5, pp. 1343–1365, Mar. 2020.

[27] S. W. Running, R. R. Nemani, F. A. Heinsch, M. Zhao, M. Reeves, and H. Hashimoto, "A continuous satellite-derived measure of global terrestrial primary production," *BioScience*, vol. 54, no. 6, pp. 547–560, Jun. 2004.

[28] C. Jiang and Y. Ryu, "Multi-scale evaluation of global gross primary productivity and evapotranspiration products derived from breathing Earth system simulator (BESS)," *Remote Sens. Environ.*, vol. 186, pp. 528–547, Dec. 2016.

[29] M. Jung *et al.*, "Global patterns of land-atmosphere fluxes of carbon dioxide, latent heat, and sensible heat derived from eddy covariance, satellite, and meteorological observations," *J. Geophys. Res.*, vol. 116, pp. 1–16, Sep. 2011.

[30] G. Tramontana *et al.*, "Predicting carbon dioxide and energy fluxes across global FLUXNET sites with regression algorithms," *Biogeosciences*, vol. 13, no. 14, pp. 4291–4313, Jul. 2016.

[31] P. Bodesheim, M. Jung, F. Gans, M. D. Mahecha, and M. Reichstein, "Upscaled diurnal cycles of land–atmosphere fluxes: A new global half-hourly data product," *Earth Syst. Sci. Data*, vol. 10, no. 3, pp. 1327–1365, Jul. 2018.

[32] G. Badgley, C. B. Field, and J. A. Berry, "Canopy near-infrared reflectance and terrestrial photosynthesis," *Sci. Adv.*, vol. 3, no. 3, Mar. 2017, Art. no. e1602244.

[33] G. Badgley, L. D. L. Anderegg, J. A. Berry, and C. B. Field, "Terrestrial gross primary production: Using NIRV to scale from site to globe," *Global Change Biol.*, vol. 25, no. 11, pp. 3731–3740, 2019.

[34] G. Camps-Valls *et al.*, "A unified vegetation index for quantifying the terrestrial biosphere," *Sci. Adv.*, vol. 7, no. 9, Feb. 2021, Art. no. eabc7447.

[35] X. Ma *et al.*, "Monitoring plant functional diversity using the reflectance and echo from space," *Remote Sens.*, vol. 12, no. 8, p. 1248, Apr. 2020.

[36] Y. Zhang, M. Migliavacca, J. Penuelas, and W. Ju, "Advances in hyperspectral remote sensing of vegetation traits and functions," *Remote Sens. Environ.*, vol. 252, Jan. 2021, Art. no. 112121.

[37] R. Fernandez-Beltran, F. Pla, J. Kang, J. Moreno, and A. Plaza, "Sentinel-3/FLEX biophysical product confidence using Sentinel-2 land-cover spatial distributions," *IEEE J. Sel. Topics Appl. Earth Observ. Remote Sens.*, vol. 14, pp. 3447–3461, 2021.

[38] X. Ma *et al.*, "Inferring plant functional diversity from space: The potential of Sentinel-2," *Remote Sens. Environ.*, vol. 233, Nov. 2019, Art. no. 111368.

[39] W. J. Frampton, J. Dash, G. Watmough, and E. J. Milton, "Evaluating the capabilities of Sentinel-2 for quantitative estimation of biophysical variables in vegetation," *ISPRS J. Photogramm. Remote Sens.*, vol. 82, pp. 83–92, Aug. 2013.

[40] R. Darvishzadeh *et al.*, "Mapping leaf chlorophyll content from Sentinel-2 and RapidEye data in spruce stands using the invertible forest reflectance model," *Int. J. Appl. Earth Observ. Geoinf.*, vol. 79, pp. 58–70, Jul. 2019.

[41] T. W. Gara, R. Darvishzadeh, A. K. Skidmore, T. Wang, and M. Heurich, "Accurate modelling of canopy traits from seasonal Sentinel-2 imagery based on the vertical distribution of leaf traits," *ISPRS J. Photogramm. Remote Sens.*, vol. 157, pp. 108–123, Nov. 2019.

[42] A. M. Ali *et al.*, "Comparing methods for mapping canopy chlorophyll content in a mixed mountain forest using Sentinel-2 data," *Int. J. Appl. Earth Observ. Geoinf.*, vol. 87, May 2020, Art. no. 102037.

[43] A. Wolanin *et al.*, "Estimating crop primary productivity with Sentinel-2 and Landsat 8 using machine learning methods trained with radiative transfer simulations," *Remote Sens. Environ.*, vol. 225, pp. 441–457, May 2019.

[44] S. Lin, J. Li, Q. Liu, L. Li, J. Zhao, and W. Yu, "Evaluating the effectiveness of using vegetation indices based on red-edge reflectance from Sentinel-2 to estimate gross primary productivity," *Remote Sens.*, vol. 11, no. 11, p. 1303, May 2019.

[45] Z. Cai *et al.*, "Modelling daily gross primary productivity with Sentinel-2 data in the Nordic region–comparison with data from MODIS," *Remote Sens.*, vol. 13, no. 3, p. 469, Jan. 2021.

[46] M. Main-Knorn, B. Pflug, J. Louis, V. Debaecker, U. Müller-Wilm, and F. Gascon, "Sen2Cor for Sentinel-2," *Proc. SPIE*, vol. 10427, Oct. 2017, Art. no. 1042704.

[47] *SNAP–ESA Sentinel Application Platform*, Brockmann Consult, SkyWatch, and C-S, Hamburg, Germany, 2020.

[48] R. E. Shiffler, "Maximum Z scores and outliers," *Amer. Statist.*, vol. 42, no. 1, pp. 79–80, Feb. 1988, doi: 10.1080/00031305.1988.10475530.

[49] R. B. Cleveland, W. S. Cleveland, J. E. McRae, and I. Terpenning, "STL: A seasonal-trend decomposition," *J. Off. Statist.*, vol. 6, no. 1, pp. 3–73, 1990.

[50] M. Dancho and D. Vaughan, *Anomalize: Tidy Anomaly Detection*, R Package, 2020.

[51] N. V. Chawla, K. W. Bowyer, L. O. Hall, and W. P. Kegelmeyer, "SMOTE: Synthetic minority over-sampling technique," *J. Artif. Intell. Res.*, vol. 16, pp. 321–357, Jun. 2002.

[52] L. Torgo, R. P. Ribeiro, B. Pfahringer, and P. Branco, "SMOTE for regression," in *Progress in Artificial Intelligence*, L. Correia, L. P. Reis, and J. Cascalho, Eds. Berlin, Germany: Springer, 2013, pp. 378–389.

[53] P. Branco, L. Torgo, and R. P. Ribeiro, "SMOGN: A pre-processing approach for imbalanced regression," in *Proc. 1St Int. Workshop Learn. With Imbalanced Domains, Theory Appl.*, 2017, pp. 36–50.

[54] H. Meyer, C. Reudenbach, T. Hengl, M. Katurji, and T. Nauss, "Improving performance of spatio-temporal machine learning models using forward feature selection and target-oriented validation," *Environ. Model. Softw.*, vol. 101, pp. 1–9, Mar. 2018.

[55] H. Meyer, *CAST: 'Caret' Applications for Spatial-Temporal Models*, R Package, 2020.

[56] F. Wilcoxon, "Individual Comparisons by Ranking Methods," *Biometrics Bull.*, vol. 1, no. 6, pp. 80–83, 1945.

[57] L. Breiman, "Random forests," *Mach. Learn.*, vol. 45, no. 1, pp. 5–32, 2001.

[58] H. Meyer, C. Reudenbach, S. Wöllauer, and T. Nauss, "Importance of spatial predictor variable selection in machine learning applications—Moving from data reproduction to spatial prediction," *Ecological Model.*, vol. 411, Nov. 2019, Art. no. 108815.

[59] H. G. Jones and R. A. Vaughan, *Remote Sensing of Vegetation: Principles, Techniques, and Applications*. Oxford, U.K.: OUP Oxford, Jul. 2010.

[60] J. R. Miller, E. W. Hare, and J. Wu, "Quantitative characterization of the vegetation red edge reflectance 1. An inverted-Gaussian reflectance model," *Int. J. Remote Sens.*, vol. 11, no. 10, pp. 1755–1773, 1990.

[61] A. Gitelson and M. N. Merzlyak, "Quantitative estimation of chlorophyll—A using reflectance spectra: Experiments with autumn chestnut and Maple leaves," *J. Photochem. Photobiol. B, Biol.*, vol. 22, no. 3, pp. 247–252, Mar. 1994.

[62] A. A. Gitelson, Y. Gritz, and M. N. Merzlyak, "Relationships between leaf chlorophyll content and spectral reflectance and algorithms for non-destructive chlorophyll assessment in higher plant leaves," *J. Plant Physiol.*, vol. 160, no. 3, pp. 271–282, 2003.

[63] J. Penuelas, F. Baret, and I. Filella, "Semi-empirical indices to assess carotenoids/chlorophyll a ratio from leaf spectral reflectance," *Photosynthetica*, vol. 31, no. 2, pp. 221–230, 1995.

[64] S. Lin *et al.*, "Improved global estimations of gross primary productivity of natural vegetation types by incorporating plant functional type," *Int. J. Appl. Earth Observ. Geoinf.*, vol. 100, Aug. 2021, Art. no. 102328.

[65] C. Albergel *et al.*, "Monitoring and forecasting the impact of the 2018 summer heatwave on vegetation," *Remote Sens.*, vol. 11, no. 5, p. 520, Mar. 2019.

[66] W. Peters, A. Bastos, P. Ciais, and A. Vermeulen, "A historical, geographical and ecological perspective on the 2018 European summer drought," *Phil. Trans. Roy. Soc. B, Biol. Sci.*, vol. 375, no. 1810, Oct. 2020, Art. no. 20190505.

[67] M. Flach, A. Brenning, F. Gans, M. Reichstein, S. Sippel, and M. D. Mahecha, "Vegetation modulates the impact of climate extremes on gross primary production," *Biogeosciences*, vol. 18, no. 1, pp. 39–53, Jan. 2021.

[68] S. Sippel *et al.*, "Drought, heat, and the carbon cycle: A review," *Current Climate Change Rep.*, vol. 4, no. 3, pp. 266–286, Sep. 2018.

[69] R. Guzinski and H. Nieto, "Evaluating the feasibility of using Sentinel-2 and Sentinel-3 satellites for high-resolution evapotranspiration estimations," *Remote Sens. Environ.*, vol. 221, pp. 157–172, Feb. 2019.

[70] M. Jung *et al.*, "The FLUXCOM ensemble of global land-atmosphere energy fluxes," *Sci. Data*, vol. 6, no. 1, pp. 1–14, May 2019.

[71] D. Zanaga *et al.*, "ESA WorldCover 10 m 2020 V100," Zenodo, Oct. 2021, doi: 10.5281/zenodo.5571936.

[72] S. Bolívar-Santamaría and B. Reu, "Detection and characterization of agroforestry systems in the Colombian Andes using Sentinel-2 imagery," *Agroforestry Syst.*, vol. 95, no. 3, pp. 499–514, Mar. 2021.

[73] C. Ludwig, R. Hecht, S. Lautenbach, M. Schorcht, and A. Zipf, "Mapping public urban green spaces based on OpenStreetMap and Sentinel-2 imagery using belief functions," *ISPRS Int. J. Geo-Geoinf.*, vol. 10, no. 4, p. 251, Apr. 2021.

[74] A. Carrara, I. A. Janssens, J. Curiel Yuste, and R. Ceulemans, "Seasonal changes in photosynthesis, respiration and NEE of a mixed temperate forest," *Agricult. Forest Meteorol.*, vol. 126, nos. 1–2, pp. 15–31, Nov. 2004.

[75] C. Moureaux, A. Debacq, B. Bodson, B. Heinesch, and M. Aubinet, "Annual net ecosystem carbon exchange by a sugar beet crop," *Agricult. Forest Meteorol.*, vol. 139, nos. 1–2, pp. 25–39, Sep. 2006.

[76] M. Aubinet, B. Chermanne, M. Vandenhaute, B. Longdoz, M. Yernaux, and E. Laitat, "Long term carbon dioxide exchange above a mixed forest in the Belgian ardennes," *Agricult. Forest Meteorol.*, vol. 108, no. 4, pp. 293–315, Jul. 2001.

[77] L. Merbold, W. Eugster, J. Stieger, M. Zahniser, D. Nelson, and N. Buchmann, "Greenhouse gas budget (CO_2, CH_4 and N_2O) of intensively managed grassland following restoration," *Global Change Biol.*, vol. 20, no. 6, pp. 1913–1928, Jun. 2014.

[78] S. Zielis, S. Etzold, R. Zweifel, W. Eugster, M. Haeni, and N. Buchmann, "NEP of a Swiss subalpine forest is significantly driven not only by current but also by previous year's weather," *Biogeosciences*, vol. 11, no. 6, pp. 1627–1635, Mar. 2014.

[79] D. Imer, L. Merbold, W. Eugster, and N. Buchmann, "Temporal and spatial variations of soil CO_2, CH_4 and N_2O fluxes at three differently managed grasslands," *Biogeosciences*, vol. 10, no. 9, pp. 5931–5945, Sep. 2013.

[80] S. Etzold *et al.*, "The carbon balance of two contrasting mountain forest ecosystems in Switzerland: Similar annual trends, but seasonal differences," *Ecosystems*, vol. 14, no. 8, pp. 1289–1309, Dec. 2011.

[81] D. Dietiker, N. Buchmann, and W. Eugster, "Testing the ability of the DNDC model to predict CO_2 and water vapour fluxes of a Swiss cropland site," *Agricult., Ecosyst. Environ.*, vol. 139, no. 3, pp. 396–401, Nov. 2010.

[82] M. Acosta *et al.*, "Soil surface CO_2 efflux measurements in Norway spruce forests: Comparison between four different sites across Europe—From boreal to Alpine forest," *Geoderma*, vol. 192, pp. 295–303, Jan. 2013.

[83] J. Dušek, H. Čížková, S. Stellner, R. Czerný, and J. Květ, "Fluctuating water table affects gross ecosystem production and gross radiation use efficiency in a sedge-grass Marsh," *Hydrobiologia*, vol. 692, no. 1, pp. 57–66, Aug. 2012.

[84] P. M. Anthoni *et al.*, "Forest and agricultural land-use-dependent CO_2 exchange in Thuringia, Germany," *Global Change Biol.*, vol. 10, no. 12, pp. 2005–2019, Dec. 2004.

[85] A.-K. Prescher, T. Grünwald, and C. Bernhofer, "Land use regulates carbon budgets in eastern Germany: From NEE to NBP," *Agricult. Forest Meteorol.*, vol. 150, nos. 7–8, pp. 1016–1025, Jul. 2010.

[86] A. Knohl, E.-D. Schulze, O. Kolle, and N. Buchmann, "Large carbon uptake by an unmanaged 250-year-old deciduous forest in central Germany," *Agricult. Forest Meteorol.*, vol. 118, nos. 3–4, pp. 151–167, Sep. 2003.

[87] H. Post, H. J. Hendricks Franssen, A. Graf, M. Schmidt, and H. Vereecken, "Uncertainty analysis of eddy covariance CO_2 flux measurements for different EC tower distances using an extended two-tower approach," *Biogeosciences*, vol. 12, no. 4, pp. 1205–1221, Feb. 2015.

[88] M. Mauder *et al.*, "A strategy for quality and uncertainty assessment of long-term eddy-covariance measurements," *Agricult. Forest Meteorol.*, vol. 169, pp. 122–135, Feb. 2013.

[89] T. GrüNwald and C. Bernhofer, "A decade of carbon, water and energy flux measurements of an old spruce forest at the anchor station tharandt," *Tellus B, Chem. Phys. Meteorol.*, vol. 59, no. 3, pp. 387–396, Jan. 2007.

[90] K. Pilegaard, A. Ibrom, M. S. Courtney, P. Hummelshøj, and N. O. Jensen, "Increasing net CO_2 uptake by a Danish beech forest during the period from 1996 to 2009," *Agricult. Forest Meteorol.*, vol. 151, no. 7, pp. 934–946, Jul. 2011.

[91] T. S. El-Madany *et al.*, "Drought and heatwave impacts on semi-arid ecosystems' carbon fluxes along a precipitation gradient," *Phil. Trans. Roy. Soc. B, Biol. Sci.*, vol. 375, no. 1810, Oct. 2020, Art. no. 20190519.

[92] Y. Luo *et al.*, "Using near-infrared-enabled digital repeat photography to track structural and physiological phenology in Mediterranean Tree–Grass ecosystems," *Remote Sens.*, vol. 10, no. 8, p. 1293, Aug. 2018.

[93] M. Koskinen, K. Minkkinen, P. Ojanen, M. Kämäräinen, T. Laurila, and A. Lohila, "Measurements of CO_2 exchange with an automated chamber system throughout the year: Challenges in measuring night-time respiration on porous peat soil," *Biogeosciences*, vol. 11, no. 2, pp. 347–363, Jan. 2014.

[94] L. Vitale, P. Di Tommasi, G. D'Urso, and V. Magliulo, "The response of ecosystem carbon fluxes to LAI and environmental drivers in a maize crop grown in two contrasting seasons," *Int. J. Biometeorol.*, vol. 60, no. 3, pp. 411–420, Mar. 2016.

[95] M. Galvagno *et al.*, "Phenology and carbon dioxide source/sink strength of a subalpine grassland in response to an exceptionally short snow season," *Environ. Res. Lett.*, vol. 8, no. 2, Apr. 2013, Art. no. 025008.

[96] E. J. Moors, "Water use of forests in The Netherlands," Vrije Universiteit, Amsterdam, The Netherlands, Tech. Rep. 41, 2012.

[97] I. M. Milyukova, O. Kolle, A. V. Varlagin, N. N. Vygodskaya, E.-D. Schulze, and J. Lloyd, "Carbon balance of a southern Taiga spruce stand in European Russia," *Tellus B: Chem. Phys. Meteorol.*, vol. 54, no. 5, pp. 429–442, Nov. 2002.

[98] J. Kurbatova, C. Li, A. Varlagin, X. Xiao, and N. Vygodskaya, "Modeling carbon dynamics in two adjacent spruce forests with different soil conditions in Russia," *Biogeosciences*, vol. 5, no. 4, pp. 969–980, Jul. 2008.

[99] M. L. Fischer, D. P. Billesbach, J. A. Berry, W. J. Riley, and M. S. Torn, "Spatiotemporal variations in growing season exchanges of CO_2, H_2O, and sensible heat in agricultural fields of the southern great plains," *Earth Interact.*, vol. 11, no. 17, pp. 1–21, Oct. 2007.
[100] A. P. Ouimette *et al.*, "Carbon fluxes and interannual drivers in a temperate forest ecosystem assessed through comparison of top-down and bottom-up approaches," *Agricult. Forest Meteorol.*, vols. 256–257, pp. 420–430, Jun. 2018, doi: 10.1016/j.agrformet.2018.03.017.
[101] H. Chu *et al.*, "Representativeness of eddy-covariance flux footprints for areas surrounding AmeriFlux sites," *Agricult. Forest Meteorol.*, vols. 301–302, p. 108350, May 2021, doi: 10.1016/j.agrformet.2021.108350.
[102] D. T. Roman, K. A. Novick, E. R. Brzostek, D. Dragoni, F. Rahman, and R. P. Phillips, "The role of isohydric and anisohydric species in determining ecosystem-scale response to severe drought," *Oecologia*, vol. 179, no. 3, pp. 641–654, Nov. 2015, doi: 10.1007/s00442-015-3380-9.
[103] M. Litvak, "AmeriFlux U.S.-Seg sevilleta grassland from 2007-present," Tech. Rep., 2016.
[104] M. Litvak, "AmeriFlux U.S.-Ses sevilleta shrubland from 2007-present," Tech. Rep., 2016.
[105] C. M. Gough, *et al.*, "Sustained carbon uptake and storage following moderate disturbance in a great lakes forest," *Ecol. Appl.*, vol. 23, no. 5, pp. 1202–1215, 2013.
[106] M. Litvak, "AmeriFlux U.S.-Vcm valles caldera mixed conifer from 2007-Present," Tech. Rep., 2016.
[107] M. Litvak, "AmeriFlux U.S.-Wjs willard juniper savannah from 2007-present," Tech. Rep., 2016.
[108] Y. J. Kaufman and D. Tanre, "Atmospherically resistant vegetation index (ARVI) for EOS-MODIS," *IEEE Trans. Geosci. Remote Sens.*, vol. 30, no. 2, pp. 261–270, Mar. 1992.
[109] C. J. Tucker, "Remote sensing of leaf water content in the near infrared," *Remote Sens. Environ.*, vol. 10, no. 1, pp. 23–32, Aug. 1980.
[110] B. Pinty and M. M. Verstraete, "GEMI: A non-linear index to monitor global vegetation from satellites," *Vegetatio*, vol. 101, no. 1, pp. 15–20, Jul. 1992.
[111] A. A. Gitelson, Y. J. Kaufman, and M. N. Merzlyak, "Use of a green channel in remote sensing of global vegetation from EOS-MODIS," *Remote Sens. Environ.*, vol. 58, no. 3, pp. 289–298, 1996.
[112] R. E. Crippen, "Calculating the vegetation index faster," *Remote Sens. Environ.*, vol. 34, no. 1, pp. 71–73, 1990.
[113] C. S. T. Daughtry, C. L. Walthall, M. S. Kim, E. B. de Colstoun, and J. E. McMurtrey, III, "Estimating corn leaf chlorophyll concentration from leaf and canopy reflectance," *Remote Sens. Environ.*, vol. 74, no. 2, pp. 229–239, Nov. 2000.
[114] J. Qi, A. Chehbouni, A. R. Huete, Y. H. Kerr, and S. Sorooshian, "A modified soil adjusted vegetation index," *Remote Sens. Environ.*, vol. 48, no. 2, pp. 119–126, 1994.
[115] J. Dash and P. J. Curran, "The MERIS terrestrial chlorophyll index," *Int. J. Remote Sens.*, vol. 25, no. 23, pp. 5403–5413, Dec. 2004.
[116] J. Delegido, J. Verrelst, L. Alonso, and J. Moreno, "Evaluation of sentinel-2 red-edge bands for empirical estimation of green LAI and chlorophyll content," *Sensors*, vol. 11, no. 7, pp. 7063–7081, 2011.
[117] G. A. Blackburn, "Quantifying chlorophylls and caroteniods at leaf and canopy scales: An evaluation of some hyperspectral approaches," *Remote Sens. Environ.*, vol. 66, no. 3, pp. 273–285, Dec. 1998.
[118] A. J. Richardson and C. L. Wiegand, "Distinguishing vegetation from soil background information," *Photogramm. Eng. Remote Sens.*, vol. 43, no. 12, pp. 1541–1552, Dec. 1977.
[119] D. J. Major, F. Baret, and G. Guyot, "A ratio vegetation index adjusted for soil brightness," *Int. J. Remote Sens.*, vol. 11, no. 5, pp. 727–740, May 1990.
[120] G. Guyot and F. Baret, "Utilisation de la haute resolution spectrale pour suivre l'etat des couverts vegetaux," in *Spectral Signatures of Objects in Remote Sensing*, vol. 287, Apr. 1988, p. 279.
[121] A. R. Huete, "A soil-adjusted vegetation index (SAVI)," *Remote Sens. Environ.*, vol. 25, no. 3, pp. 295–309, 1988.
[122] G. M. Senseman, C. F. Bagley, and S. A. Tweddale, "Correlation of rangeland cover measures to satellite-imagery-derived vegetation indices," *Geocarto Int.*, vol. 11, no. 3, pp. 29–38, Sep. 1996.
[123] F. Baret, G. Guyot, and D. J. Major, "TSAVI: A vegetation index which minimizes soil brightness effects on LAI and APAR estimation," in *Proc. 12th Can. Symp. Remote Sens. Geosci. Remote Sens. Symp.*, Jul. 1989, pp. 1355–1358.
[124] J. G. P. W. Clevers, "The derivation of a simplified reflectance model for the estimation of leaf area index," *Remote Sens. Environ.*, vol. 25, no. 1, pp. 53–69, Jun. 1988.
[125] A. A. Gitelson *et al.*, "Relationship between gross primary production and chlorophyll content in crops: Implications for the synoptic monitoring of vegetation productivity," *J. Geophys. Res.*, vol. 111, no. D8, 2006, Art. no. D08S11.
[126] A. A. Gitelson, A. Viña, T. J. Arkebauer, D. C. Rundquist, G. Keydan, and B. Leavitt, "Remote estimation of leaf area index and green leaf biomass in maize canopies," *Geophys. Res. Lett.*, vol. 30, no. 5, p. 1248, Mar. 2003.
[127] J. Rouse Jr., R. Haas, J. Schell, and D. Deering, "Paper a 20," in *Proc. 3rd Earth Resour. Technol. Satellite Symp. Symposium Held Goddard Space Flight Center Washington, Prepared Goddard Space Flight Center*, vol. 351. Washington, DC, USA: Scientific and Technical Information Office, National Aeronautics and Space, 1974, p. 309.

Daniel E. Pabon-Moreno received the B.Sc. degree in biology from the Industrial University of Santander, Bucaramanga, Colombia, in 2017. He is currently pursuing the Ph.D. degree with Friedrich Schiller University Jena, Jena, Germany.

He is currently with the Department Biogeochemical Integration, Max Planck Institute for Biogeochemistry, Jena. His research interests include vegetation response to climate change, ecosystem monitoring using remote sensing information, and ecosystem physiophenology modeling using circular statistics.

Mirco Migliavacca received the Ph.D. degree from the University of Milano-Bicocca, Milan, Italy, in 2009.

He worked as a postdoc with the European Commission and then as a Group Leader with the Max Planck Institute for Biogeochemistry, Jena, Germany. He is currently an Environmental Scientist with the University of Milano-Bicocca. Currently, he is a Scientific Officer with the European Commission, Joint Research Centre. His research interests involve broad questions in the fields of global change ecology, biometeorology, and biogeochemistry related to the carbon and water cycles in terrestrial ecosystems and climate–biosphere interactions.

Markus Reichstein received the Ph.D. degree from the Department of Plant Ecology, University of Bayreuth, Bayreuth, Germany, in 2001.

Since 2013, he has been a Professor of global geoecology with Friedrich Schiller University, Jena, Germany, and the Founding Director of the Michael Stifel Center Jena for Data-Driven and Simulation Science. He is currently the Director of the Biogeochemical Integration Department, Max Planck Institute for Biogeochemistry, Jena. His research interests include around the response and feedback of ecosystems (vegetation and soils) to climatic variability with an Earth system perspective, considering coupled carbon, water, and nutrient cycles, as well as specific interest in the interplay of climate extremes with ecosystem and societal resilience.

Dr. Reichstein has been serving as a Lead Author for the IPCC Special Report on Climate Extremes (SREX) and a member for the German Committee Future Earth on Sustainability Research and Thuringian Panel on Climate.

Miguel D. Mahecha received the Ph.D. degree from ETH Zürich, Zürich, Switzerland, in 2009.

He was a Group Leader with the Max Planck Institute for Biogeochemistry, Jena, Germany. Since 2020, he has been a Full Professor with the Remote Sensing Centre for Earth System Research, Leipzig University, and the Helmholtz Centre for Environmental Research, UFZ, Germany. His research interests revolve around global ecosystem responses to climate variability with an emphasis on the role of climate extremes. He also works on quantifying biodiversity patterns, and he has a genuine interest in Earth system data science methods.